Journal of Molecular Spectroscopy 392 (2023) 111743

Contents lists available at ScienceDirect

Journal of Molecular Spectroscopy

journal homepage: www.elsevier.com/locate/yjmsp

High-resolution rovibrational spectroscopy of *trans*-formic acid in the ν_1 OH stretching fundamental: Dark state coupling and evidence for charge delocalization dynamics

Ya-Chu Chan [a,b], David J. Nesbitt [a,b,c,*]

[a] JILA, University of Colorado Boulder and National Institute of Standards and Technology, Boulder, CO 80309, USA
[b] Department of Chemistry, University of Colorado Boulder, Boulder, CO 80309, USA
[c] Department of Physics, University of Colorado Boulder, Boulder, CO 80309, USA

ARTICLE INFO

Keywords:
Formic acid
PGOPHER
High-resolution spectroscopy
Infrared spectroscopy
Supersonic expansion
Fermi resonance

ABSTRACT

High-resolution infrared (IR) reduced-Doppler absorption spectra of jet-cooled gas phase *trans*-formic acid in the ν_1 OH stretching fundamental region are reported for the first time, obtained by supersonically expanding *trans*-formic acid/Ar mixtures through a slit jet nozzle source and rotationally cooling to $T_{rot} \approx 10.9(5)$ K, with absorption signals recorded by high-resolution difference-frequency IR absorption spectroscopy. Two *a*/*b*-type rovibrational bands of comparable intensity, one ~10-fold weaker *b*-type band, and one ~6-fold weaker *a*-type band are observed, with vibrational band origins at 3570.493(5), 3566.793(5), 3560.032(9), and 3534.6869(2) cm^{-1}, respectively. Based on previous Raman jet spectroscopic work by Nejad and Sibert [A. Nejad, E.L. Sibert III, The Raman jet spectrum of *trans*-formic acid and its deuterated isotopologs: Combining theory and experiment to extend the vibrational database, J. Chem. Phys. 154(6) (2021) 064301.], these four rovibrational bands have been assigned to ν_1, $(\nu_2 + \nu_7)$, $(\nu_6 + 2\nu_7 + 2\nu_9)$, and $2\nu_3$, respectively. Specifically, two of the three upper dark states ($2^1 7^1$ (a') and $6^1 7^2 9^2$ (a')) are close enough to the "bright" 1^1 (a') state to facilitate strong anharmonic resonance interactions, which results in intensity mixing into the two zero-order bands that would otherwise be "dark". Furthermore, our high-resolution spectral analysis reveals that there are local rotational crossings between these zero-order 1^1 and $2^1 7^1$ states resulting in extra lines (i.e., some upper levels in the nominally ν_1 band have majority zero-order $2^1 7^1$ state character). This motivates development of a 3 coupled state (1^1, $2^1 7^1$, and $6^1 7^2 9^2$) picture to aid in the spectral analysis, which is able to match all 3 observed band origins and relative band intensities, as well as indicate the necessity of multistate (> 2) coupling. Though limited by range of J and K_a levels ($J' \leq 9$ and $K_a' \leq 3$) populated at supersonic jet temperatures, this work offers first precision spectroscopic analysis of *trans*-formic acid in the ν_1 OH stretch region, which should aid in assignment of the more complete yet highly congested room temperature FTIR spectra [D. Hurtmans, F. Herregodts, M. Herman, J. Liévin, A. Campargue, A. Garnache, A. Kachanov, Spectroscopic and ab initio investigation of the ν_{OH} overtone excitation in *trans*-formic acid, J. Chem. Phys. 113(4) (2000) 1535–1545.]. Finally, and in sharp contrast to the spectral complexity in the three predominantly *b*-type bands, the lone *a*-type $2\nu_3$ rovibrational band at 3534.6869(2) cm^{-1} is well described by a simple, rigid asymmetric top Hamiltonian.

1. Introduction

As the simplest carboxylic acid, formic acid (HCOOH) plays a dominant role in atmospheric chemistry of the troposphere regime, with particularly important terrestrial impact on the pH of precipitation and "acid rain" phenomena [1,2]. By virtue of its structural simplicity and exclusive synthesis from first row elements, *trans*-formic acid is thought to play a key role in interstellar chemistry [3–5]. Indeed, evidence for the existence of formic acid in the interstellar medium was reported by microwave astronomers in the early 1970's [6,7], and since then, by microwave methods in many sources such as cold dark clouds [8], hot molecular cores [5], and comets [9]. In addition to atmospheric and astrochemical relevance, formic acid is of particular dynamical interest as the result of an isomerization double well between the *trans* and *cis*

* Corresponding author at: JILA, University of Colorado Boulder and National Institute of Standards and Technology, Boulder, CO 80309, USA
E-mail address: djn@jila.colorado.edu (D.J. Nesbitt).

https://doi.org/10.1016/j.jms.2023.111743
Received 8 November 2022; Received in revised form 13 January 2023; Accepted 16 January 2023
Available online 21 January 2023

formic acid rotamers (see Fig. 1). Due to the delocalization of π-electrons over the heavy atom COO framework, both rotamers have planar equilibrium geometries with C_s symmetry, with *trans*-formic acid (and the much higher energy *cis*-isomer) has two hydrogen atoms on opposite (same) sides of the C−O bond, respectively. From first equilibrium microwave measurements of the *cis*-rotamer, the energy difference between ground vibrational states of the two rotamers was estimated to be 1365(30) cm^{-1}, with a ~ 4827 cm^{-1} barrier to internal rotation [10]. As a result, the *trans*-rotamer is predicted to be ≈ 1000 times more abundant than the *cis*-rotamer at room temperature, with completely negligible equilibrium populations at much lower temperature conditions of the interstellar medium. Thus, the detection of both *cis* and *trans* formic acid in interstellar planetary forming regions via microwave spectroscopy provides indisputable evidence for *highly non-equilibrium* internal rotational dynamics of these two isomers in a strongly asymmetric double minimum potential [11].

There have of course also been extensive terrestrial studies on formic acid with microwave and far-infrared spectroscopy instruments [3,10,12,13]. Specifically, Fourier transform far-infrared, submillimeter, and millimeter spectra of *cis*- and *trans*-HCOOH and *trans*-$H^{13}COOH$ have been recorded by Winnewisser *et al.* [14], providing precision ground state rotational and centrifugal distortion constants to aid in the assignment (*vide infra*) of current high-resolution rovibrational spectra in the infrared. With regard to facilitating such infrared spectroscopic studies, experimental and theoretical predictions for the 3 N – 6 = 9 fundamental vibrational modes of *trans*- and *cis*-formic acid rotamers are summarized in Table 1. High-resolution spectra of *trans*-rotamer have been obtained using laser-microwave double and triple resonance techniques [15] and Fourier transform spectroscopy [16–18], yielding spectroscopic constants for all nine fundamental modes, except ν_1, ν_4 and ν_5. The vibrationally excited states of the corresponding *cis*-rotamer, on the other hand, have received far less attention. This is due to the exceedingly low *cis* to *trans* population ratios under typical thermal conditions, which therefore require the use of much more highly sensitive techniques. So far, high-resolution spectra have been reported for ν_9 OH torsional mode [19] and only quite recently for the ν_1 OH stretch mode [20]. For the remaining *cis*-formic acid normal modes, only low resolution vibrational assignments in the gas-phase [21] and Ar matrix [22] have been possible, with the sole exception being lack of low resolution detection of the ν_8 CH wagging mode.

Beyond fundamentals, IR overtone spectroscopy can be particularly powerful in providing spectral information on chemically significant regions of the full 9D potential surface, at energies relevant to unimolecular and bimolecular collision processes as well as intra- and intermolecular energy redistribution [23,24]. Previous overtone spectroscopic studies have enabled a deeper understanding of the isomerization dynamics and possible bond-selective chemistry of formic acid [25,26]. High-resolution absorption spectra of the more abundant *trans*-formic acid have been recorded under room temperature conditions between 626.16 cm^{-1} to 13,284.1 cm^{-1} by Fourier transform spectroscopy and intracavity laser absorption spectroscopy [27]. A total of 62 bands from ν_7 (626.16 cm^{-1}) up to $4\nu_1$ (13,284.08 cm^{-1}) have been observed and assigned, yielding band origins, vibrational frequency differences, band intensities, and effective vibrational constants. For the $n\nu_2$ CH stretching mode ($n = 2 - 4$), unfortunately, broad structureless overtone absorption due to the very strongly H-bonded formic acid dimer overlaps and obscures the more highly resolved CH stretch features of the monomer. By way of contrast, the corresponding OH stretch series $n\nu_1$ ($n = 2 - 4$) for the *trans* dimer bands are strongly red-shifted due to hydrogen bonding, thus allowing the *trans* monomer study of sequential overtone OH stretches. In particular, the studies provide evidence for a progressive vibrationally-induced shift in the hydrogen from one oxygen to the other (i.e., intramolecular "proton transfer"), as indicated by evolution of the relative *a*- to *b*-type sub-band intensities. Quite recently, the $2\nu_1$ OH stretching overtone region was revisited under jet-cooled conditions (T_{rot} = 37 K) [24], where the reduced-Doppler spectra are far better resolved compared to the previous room temperature studies.

Curiously, while *overtone* spectroscopic studies of *trans*-formic acid in the OH stretch region ($n\nu_1$, $n = 2 - 4$) have been extensively studied, similarly detailed information on the OH stretch *fundamental* (ν_1) has remained surprisingly elusive, though not for lack of experimental effort. For example, the gas phase ν_1 rovibrational band spectrum was recorded with Fourier transform infrared (FTIR) methods back in 2000 [23]. Unfortunately, however, the spectra under room temperature conditions proved to be highly congested, which restricted any more detailed rotational analysis efforts. Shortly afterwards in 2002, Madeja *et al.* reported rotationally resolved ν_1 band spectra of *trans*-formic acid in helium nanodroplets at ~0.37 K [28]. Both Fermi and Coriolis interactions of 1^1 with 2^17^1 and 2^19^1 states were identified, providing further clues for the spectral congestion in gas phase room temperature spectrum. More recently in 2021, vibrational Raman jet spectrum of *trans*-formic acid in the ν_1 region was reported by Nejad and Sibert [29], with the ν_1 band at 3570 cm^{-1} and additional satellites at 3609, 3567, and 3559 cm^{-1} observed. While the band at 3567 cm^{-1} was assigned to ($\nu_2 + \nu_7$) and confirmed by sensitivity to CD vs. CH isotopic substitution, the other two bands were left unassigned. Indeed, even with the advantages provided by these additional studies, gas phase high-resolution room-temperature spectroscopy of the ν_1 band has remained unassigned for over two decades. This clearly represents an experimental challenge and opportunity for slit jet supersonic expansion laser absorption methods, which forms the primary focus of the present work. Specifically, high-resolution spectra in the ν_1 OH stretch rovibrational band

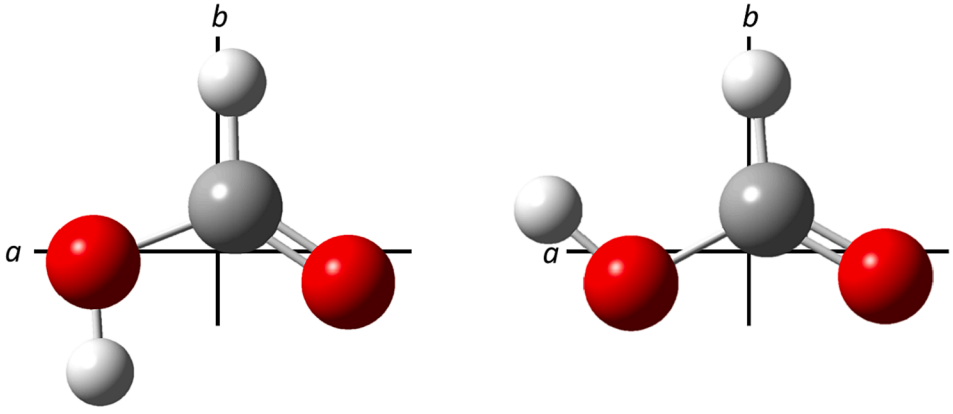

Fig. 1. The CCSD(T)/ANO2 equilibrium structures of two formic acid rotamers, *trans* (left) and *cis* (right). Note that the OH bond in *trans*-formic acid lies 7.6° away from the *b* principal rotation axis, predicting predominant *b*-type transition intensity in the ν_1 OH stretching fundamental band based on a simple bond dipole model (see Section 4.3 for details).

Table. 1
Experimental and theoretical frequencies (in cm^{-1}) of the nine normal modes of *trans*- and *cis*-formic acid. CCSD(T)/ANO2 with VPT2 level of theory is used to compute *ab initio* anharmonic frequencies and anharmonic intensity (in km/mol).

			trans-HCOOH				*cis*-HCOOH			
Mode			Experimental Freq.	Ref.[a]	Anharmonic Freq.	Anharmonic intensity[b]	Experimental Freq.	Ref.[a]	Anharmonic Freq.	Anharmonic intensity
ν_1		O − H str.	3570.493 (5)	This work	3573.5	58	3637.1571(3)	[20]	3641.2	69
ν_2		C − H str.	2942.06(1)	[15]	2930.0	19	2873(2)	[21]	2871.3	59
ν_3		C=O str.	1776.8334(3)	[16]	1778.9	312 (235.2)[c]	1818(2)	[21]	1819.5	247
ν_4	a'	H − C − O bend	1380	[27]	1385.4	3	1391.8	[22]	1390.0	0.4
ν_5		C − O − H bend	1223	[27]	1218.3	6	1243.4/1248.9	[22]	1250.0	298
ν_6		C − O str.	1104.8521(2)	[17]	1104.8	253 (208.8)[d]	1093(2)	[21]	1097.5	49
ν_7		O − C=O bend	626.16561(39)	[18]	624.5	41	662.3/662.3	[22]	655.1	10
ν_8	a''	C − H wag	1033.4692(4)	[17]	1035.4	2 (2.815)[d]	–		1015.6	0.004
ν_9		O − H tor.	640.72506(39)	[18]	639.6	136	493.420509(7)	[19]	490.3	82

[a] References for the experimental frequencies.
[b] Experimental integrated band intensities are shown in parentheses for comparison with *ab initio* anharmonic intensities.
[c] See A. Perrin *et al.* [47].
[d] See A. Perrin *et al.* [48].

region (3528 cm^{-1} to 3583 cm^{-1}) have been obtained under reduced-Doppler, slit jet conditions, in which the *trans*-rotamer is cooled down to a rotational temperature of $T_{rot} \sim 11$ K. This results in a dramatic simplification of the spectra, enabling a first high-resolution rovibrational assignment and analysis.

The organization of this paper is as follows. The experimental method is briefly described in Section 2. The first jet-cooled spectrum of *trans*-rotamer in the OH stretching fundamental region is presented in Section 3, followed by rotational analysis yielding first precision spectroscopic constants for the 1^1, $2^1 7^1$, $6^1 7^2 9^2$, and 3^2 excited states. In Section 4, we present a detailed deperturbation analysis of strong anharmonic resonant interactions between the optically "bright" 1^1 state and near resonant "dark" $2^1 7^1$ and $6^1 7^2 9^2$ states. Finally, systematic changes in the OH stretch transition dipole moment direction are discussed. Conclusions and directions for further study are summarized in Section 5.

2. Experiment

The experimental apparatus, which combines a high-resolution difference-frequency IR spectrometer with a pulsed slit supersonic beam source, has been described in detail elsewhere [30]. In brief, difference frequency generation between a single mode tunable ring dye laser (Spectra-Physics 380A, Rhodamine 590 dye) and a single mode fixed frequency Argon ion laser (Spectra-Physics model 2020, 488 nm) generates narrow-band continuous-wave IR light source between 3200 and 4600 cm^{-1} with <1 MHz linewidth and 5–10 μW power levels. A 50 mm long magnesium-doped periodically poled lithium niobate (MgO:PPLN) crystal is used for the non-linear difference frequency generation and placed in an enclosed oven housing to maintain a uniform temperature (< 0.1 °C stability). A Fabry-Pérot etalon is locked onto the output of a polarization-stabilized HeNe laser and acts as an optical transfer cavity for frequency control of the Argon ion laser, with details of the transfer cavity stabilization described previously by Riedle *et al.*[31] During the scan, the Argon ion laser is locked onto a longitudinal mode of an actively stabilized Fabry-Pérot etalon while transmission fringes of the dye laser are recorded, which therefore correspond to a perfectly correlated scan in $\nu_{IR} = \nu_{Ar} - \nu_{dye}$ difference frequency. The IR light source is then split into two beams, with one beam (*reference*) directly sent to a liquid-nitrogen cooled InSb detector, and the other beam (*signal*) travelling through a 16-pass Herriott cell (absorption path length of 64 cm) along the slit direction in a vacuum chamber before being focused onto a second matched InSb detector. A homebuilt servoloop circuit subtracts the two balanced InSb detector outputs to suppress common mode amplitude noise on the IR laser light by 30 dB with a > 1 MHz bandwidth. Dye and Ar ion laser frequencies are monitored with a Michaelson interferometer and calibrated against well-known CH_4 asymmetric CH stretch transitions in the slit jet expansion [32], resulting in a frequency accuracy and precision on the order of 10 MHz (0.0003 cm^{-1}).

Formic acid (HCOOH) liquid is purchased from Sigma-Aldrich and used without further purification. An argon expansion gas is bubbled through a thermostatted formic acid liquid and then further diluted to produce a stable ~0.5–0.6% formic acid/Ar mixture before flowing into the pulsed valve stagnation region at a total backing pressure of ~240 mbar. The pulsed valve operates at a 19 Hz repetition rate, 1 ms opening duration, and with a rectangular 40 mm × 0.3 mm slit nozzle geometry. *Trans*-formic acid undergoes rapid cooling in the slit supersonic expansion and intersects the IR beam at right angles to achieve reduced-Doppler widths (FWHM) of 70 MHz (0.0023 cm^{-1}) due to natural collisional collimation along the 40 mm slit jet dimension. Data at each IR spectral frequency is averaged over 4 pulses, for a net 4 ms integrated time window per 12.5 MHz frequency step. There are several finite breaks in the recorded spectra between 3565 and 3569 cm^{-1} (Fig. 2) due to strong water absorption, which results in complete depletion of IR light. For first overtone of the carbonyl C=O stretch rovibrational band ($2\nu_3$) between 3528 and 3539 cm^{-1} (Fig. 3), we scan only regions where strong progressions are predicted.

3. Experimental spectrum and analysis

High-resolution IR absorption spectra of jet-cooled *trans*-formic acid in the ν_1 OH stretching fundamental region have been collected over a 55 cm^{-1} spectral range from 3528 cm^{-1} to 3583 cm^{-1}. Four rovibrational bands are found in this spectral window (Fig. 2 and 3), with all observed transitions out of the same *trans*-formic acid vibrational ground state, as readily verified by precision ground state combination differences generated from the microwave rotational constants of Winnewisser *et al.* [14] Vibrational band origins and rotational band structures of the four rovibrational bands are 3570.493(5) cm^{-1} and 3566.793(5) cm^{-1} (hybrid *a*/*b*- but predominantly *b*-type), 3560.032(9) cm^{-1} (nearly pure *b*-type), and 3534.6869(2) cm^{-1} (nearly pure *a*-type). The two highest-frequency *a*/*b*-type hybrid rovibrational bands are separated by only 3.700(7) cm^{-1} and have very comparable intensities. The *b*-type (ΔK_a = odd, ΔK_c = odd) and *a*-type (ΔK_a = even, ΔK_c = odd) rovibrational bands to the red have ~6- to 10-fold weaker intensity compared to the two intense *a*/*b*-type hybrid bands. Detailed rovibrational assignments and analyses of these four bands are as follows.

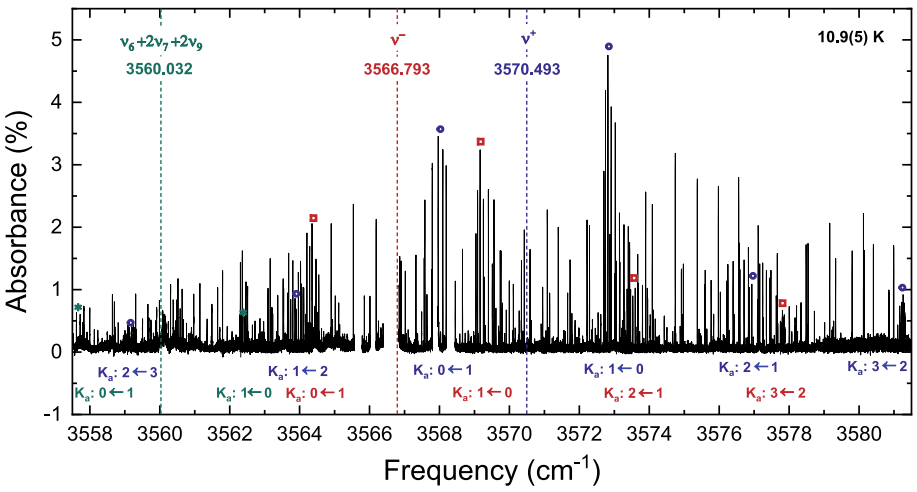

Fig. 2. Experimental absorption spectrum of jet-cooled *trans*-formic acid in the ν_1 OH stretching fundamental region, displaying three rovibrational bands with predominant *b*-type structure. The strongest progression with band origin at 3570.493 cm^{-1} is labelled ν^+ (initially assigned to ν_1) while the slightly weaker one at 3566.793 cm^{-1} is labelled ν^- (initially assigned to $\nu_2 + \nu_7$). The weakest band to the red is tentatively assign to ($\nu_6 + 2\nu_7 + 2\nu_9$). These three bands arise from anharmonic resonant interactions, where the dark combination states steal oscillator strength from the "bright" 1^1 state. The Q-branch assignments for ν^+ (indigo), ν^- (dark red), and ($\nu_6 + 2\nu_7 + 2\nu_9$) (teal) *b*-type K_a sub-bands are marked along the top and are labeled along the bottom. See text for details. (For interpretation of the references to colour in this figure legend, the reader is referred to the web version of this article.)

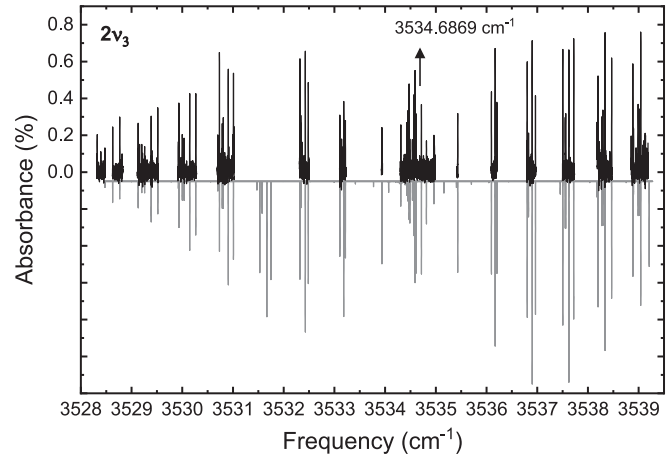

Fig. 3. Overview of CO stretch first overtone ($2\nu_3$) *a*-type rovibrational band of *trans*-formic acid. Experimental spectral regions are highly compressed in black while PGOPHER simulation is plotted downwards in gray for comparison. The band origin is at 3534.6869(2) cm^{-1}, which is ~35 cm^{-1} to the red of both ν^+ and ν^-.

3.1. The three b-type structure dominated rovibrational bands

If we assume a transition dipole moment direction of OH stretching mode along the OH bond, a predominantly *b*-type structure for the strongly infrared active ("bright") ν_1 fundamental band is expected ($\frac{\partial \mu_b}{\partial q_1} \neq 0$), as evident in Fig. 1. In addition, the vibrational band origin of the highest-frequency band seen at 3570.493(5) cm^{-1} is in very good agreement with previous room temperature FTIR work reporting ν_1 at 3570.5(1) cm^{-1} [23]. We therefore ascribe the presence of these three *b*-type predominant bands to resonant interactions between the "bright" (1^1) state and two nearby "dark" states which we endeavor to assign/interpret below (*vide infra*). The upper states involved in the three predominantly *b*-type bands must be of a' symmetry. Consequently, the symmetry of the coupling operator must also be a', which implies that resonant state mixing can arise from Fermi- (anharmonic) and/or *c*-type Coriolis interactions. Indeed, anharmonic frequencies predicted from second-order vibrational perturbation theory (VPT2) at CCSD(T)/ANO2 level of theory [33] signal the presence of several nearby dark states ($2^1 7^1$, $4^1 6^2$, and 3^2) of the correct a' symmetry to couple with the bright 1^1 state (Table 2). Our *ab initio* values are also in excellent agreement with previous anharmonic force field calculations by J. Demaison *et al.* at CCSD(T)/VTZ levels of theory [34], where cubic and quartic potential constants do predict Fermi resonance coupling between the two $1^1/2^1 7^1$ and $1^1/3^2$ pairs. Moreover, Nejad and Sibert reported vibrational eigenstates obtained from CCSD(T) potential energy surfaces [35] using high order canonical Van Vleck perturbation theory (CVPT) [36], which predict two additional "dark" states ($6^1 7^2 9^2$ and $7^3 8^1 9^1$) of a' symmetry (Table 2) [29]. Initial vibrational assignments of the three *b*-type bands are based on Nejad and Sibert from their Raman jet spectrum and theoretical calculations, from which our observed rovibrational bands at 3570.493(5) cm^{-1} and 3566.793(5) cm^{-1} are assigned as 1^1 and $2^1 7^1$, respectively, where modes ν_2 and ν_7 correspond to the C–H stretch and O–C=O bend, respectively. This previous vibrational band assignment to $2^1 7^1$ was further supported by isotopic CD substitution studies, while the band at 3560.032(9) cm^{-1} (3559 cm^{-1} in the Raman jet spectrum) was left unassigned by Nejad and Sibert. We tentatively assign this upper state to $6^1 7^2 9^2$, with ν_6 and ν_9 corresponding to C–O stretch and O–H torsional modes, respectively. Even though this postulated $6^1 7^2 9^2$ coupling ($\Delta v = 6$ and 5) with the 1^1 and $2^1 7^1$ states requires higher-order potential derivatives to be non-zero, the other possible dark states are not considered here because (i) for the $4^1 6^2$ and $7^3 8^1 9^1$ states, isotopic C–D substitution in previous Raman jet spectroscopic work excluded the ν_4 (H–C–O bend) and ν_8 (C–H wag) vibrations as coupling partners and (ii) for the 3^2 state, the vibrational band origin was already determined by Nejad and Sibert to be at 3533 cm^{-1}.

To understand how such resonant interactions affect the overall rotational structure, we have taken advantage of the powerful suite of PGOPHER programs developed by the late Colin Western for high-resolution spectral analysis [37]. As a first step, we have assigned a

Table 2
Ab initio energies (in cm^{-1}) of *trans*-formic acid vibrational levels in the OH stretching fundamental region.

Level	Γ	Vibrational energy	
		This work[a]	Nejad and Sibert[b]
1^1	a'	3573.5	3581.8
			3576.2
$2^1 7^1$	a'	3554.5	3567.8
$2^1 9^1$	a''	3567.0	–
$4^1 6^2$	a'	3571.9	3565.2
$7^3 8^1 9^1$	a'	–	3564.5
$6^1 7^2 9^2$	a'	–	3564.0
3^2	a'	3539.4	3544.9

[a] Anharmonic frequencies of all levels with up to three quanta using CCSD(T)/ANO2 with VPT2 level of theory.
[b] Energies of the vibrational eigenstates obtained from CCSD(T) potential energy surface using CVPT6. Only eigenstates with leading squared coefficients reported in this table [29].

total of 121, 109, and 22 *b*-type transitions for a "zero-order" labelling of ν_1, $(\nu_2 + \nu_7)$, and $(\nu_6 + 2\nu_7 + 2\nu_9)$ bands, respectively. In addition to predominant *b*-type progressions, both ν_1 and $(\nu_2 + \nu_7)$ bands exhibit much weaker *a*-type sub-band structure reduced in intensity by an order of magnitude (a total of 36 and 21 assigned *a*-type transitions, respectively). For the upper states involved in ν_1, $(\nu_2 + \nu_7)$, and $(\nu_6 + 2\nu_7 + 2\nu_9)$ bands, assigned transitions result in a total of 44 ($0 \leq J' \leq 9$ and $0 \leq K_a' \leq 3$), 41 ($1 \leq J' \leq 8$ and $0 \leq K_a' \leq 3$), and 12 ($1 \leq J' \leq 6$ and $0 \leq K_a' \leq 1$) upper states being measured, with center frequencies for each reported rovibrational transition listed in supplementary materials (SI). Fig. 2 displays the experimental spectrum of the three rovibrational bands, with assignments for each of the strong *b*-type K_a sub-band Q-branches reported along the bottom.

In the absence of rotational crossings between zero-order 1^1, $2^1 7^1$, and $6^1 7^2 9^2$ states, systematic energy shifts due to non-local anharmonic resonances can often be absorbed into small changes in the fitted rotational and centrifugal distortion constants. Based on this assumption, we first fit the assigned infrared transition frequencies of the three bands separately to *A*-reduced Watson Hamiltonians in the I^r representation without including any anharmonic resonance coupling. The standard deviation of the fit for the $(\nu_6 + 2\nu_7 + 2\nu_9)$ band is $\sigma = 0.0013$ cm^{-1} when all centrifugal distortion terms are fixed at zeros, which is already comparable to our measurement uncertainties (summarized in Table 3). In addition, the experimentally determined rotational constants of the $6^1 7^2 9^2$ state ($A = 2.61(1)$ cm^{-1}, $B = 0.399(2)$ cm^{-1}, and $C = 0.344(2)$ cm^{-1}) are close to CCSD(T) predictions based on vibration-rotation constants ($A = 2.6246$ cm^{-1}, $B = 0.3960$ cm^{-1}, and $C = 0.3433$ cm^{-1}), again supporting our vibrational assignment. However, for the ν_1 and $(\nu_2 + \nu_7)$ bands, the values of σ are 0.0040 cm^{-1} and 0.0178 cm^{-1}, respectively, even when three quartic centrifugal distortion constants (Δ_J, Δ_{JK}, and Δ_K) are included. These values are approximately an order of magnitude larger than our frequency measurement uncertainties, thus indicating the residual presence of local rotational crossings in the zero-order 1^1 and $2^1 7^1$ states. This is already surprising, given the low *J* and K_a rovibrational levels observed in the jet-cooled spectra. Nevertheless, this suggests close resonances between the rotational manifolds of zero-order states, which lies at the heart of the spectral challenge for previous room temperature studies by Herman and coworkers [23]. Indeed, assignment of the OH stretch fundamental for *trans*-formic acid continues to provide spectral challenges even for low supersonic jet temperatures and reduced-Doppler resolution. Simply stated, after our initial high-resolution spectral analysis, the upper states involved in the two intense *a*/*b*-type rovibrational bands *cannot* be assigned to a *global* rotational state independent admixture of zero-order 1^1 and $2^1 7^1$ states due to the presence of *local* rotational crossings reversing the majority assignment. As a result, instead of referring these two highly mixed bands by zero-order ν_1 and $(\nu_2 + \nu_7)$ notation, it will be convenient to use the more generic ν^+ and ν^- descriptors to denote relative ordering of the rovibrationally coupled states.

As a first level of effort, we briefly consider a simple 2-state model, with the same J_{K_a,K_c} levels in the zero-order 1^1 and $2^1 7^1$ states coupled through pure anharmonic vibrational mixing. Though allowed by symmetry, we neglect rotationally mediated *c*-type Coriolis interactions in this treatment, as these are generally much weaker than a low order anharmonic Fermi resonance. Quantitative extraction of the mixing between 2 rovibrational levels can be obtained by diagonalizing a 2×2 Hamiltonian matrix in a zero-order rovibrational eigenstate basis ($\varphi^0_{1^1}$ and $\varphi^0_{2^1 7^1}$) with zero-order energies ($E^0_{1^1}$ and $E^0_{2^1 7^1}$), coupled by a Fermi resonance matrix element $\beta = \left\langle \varphi^0_{1^1} | \boldsymbol{H} \varphi^0_{2^1 7^1} \right\rangle$,

$$\boldsymbol{H} = \begin{pmatrix} E^0_{1^1} & \beta \\ \beta & E^0_{2^1 7^1} \end{pmatrix} \tag{1}$$

The perturbed eigenvalues ($E^0_{1^1}$ and $E^0_{2^1 7^1}$) can be obtained from the 2×2 secular determinant of Eq. (1) and are given by,

$$E'_{1^1/2^1 7^1} = \frac{1}{2}\left[\left(E^0_{1^1} + E^0_{2^1 7^1}\right) \pm \sqrt{4\beta^2 + \Delta E^2} \right] \tag{2}$$

where ΔE is the energy separation between the zero-order states. Similarly, the perturbed eigenfunctions (Ψ'_{1^1} and $\Psi'_{2^1 7^1}$) can be expressed in terms of linear combinations of unperturbed states and the mixing angle θ,

$$\Psi'_{1^1} = cos(\theta)\varphi^0_{1^1} + sin(\theta)\varphi^0_{2^1 7^1} \tag{3}$$

$$\Psi'_{2^1 7^1} = -sin(\theta)\varphi^0_{1^1} + cos(\theta)\varphi^0_{2^1 7^1} \tag{4}$$

where θ is related to β and ΔE by,

$$tan(2\theta) = \frac{2\beta}{\Delta E} \tag{5}$$

If we further assume that only the 1^1 state is optically bright, then zero-order transition intensities of ν_1 can be expressed as,

$$I^0_{\nu_1} \propto \left| \left\langle \varphi_{ground} | \boldsymbol{\mu} \varphi^0_{1^1} \right\rangle \right|^2 \tag{6}$$

where $\boldsymbol{\mu}$ is the transition dipole moment operator. By projecting the perturbed eigenstates onto this zero-order basis, the transition intensities of the perturbed bands are given by,

$$I'_{\nu_1} \propto \left| \left\langle \varphi_{ground} | \boldsymbol{\mu} \varphi^0_{1^1} \right\rangle \left\langle \varphi^0_{1^1} | \Psi'_{1^1} \right\rangle \right|^2 = I^0_{\nu_1} cos^2(\theta) \tag{7}$$

$$I'_{(\nu_2+\nu_7)} \propto \left| \left\langle \varphi_{ground} | \boldsymbol{\mu} \varphi^0_{1^1} \right\rangle \left\langle \varphi^0_{1^1} | \Psi'_{2^1 7^1} \right\rangle \right|^2 = I^0_{\nu_1} sin^2(\theta) \tag{8}$$

From Eq. (7) and Eq. (8), the mixing angle for a specific J_{K_a,K_c} rovibrational level in the perturbed 1^1 and $2^1 7^1$ states can be obtained from relative intensities of transitions out of the same ground state to pairs of

Table 3
Experimentally determined ground and excited states rotational constants (in cm^{-1}) of *trans*-HCOOH.

		Perturbed[b,d]			(3-state system) Deperturbed[c,d]			
3-state system notation		$\|\alpha\rangle$	$\|\beta\rangle$	$\|\gamma\rangle$	$\|1\rangle$	$\|2\rangle$	$\|3\rangle$	
	Ground[a]	ν^+ (1^1)	ν^- ($2^1 7^1$)	$6^1 7^2 9^2$	1^1	$2^1 7^1$	$6^1 7^2 9^2$	3^2
A	2.58552987(4)	2.558(1)	2.5913(9)	2.61(1)	2.487(3)	2.685(3)	2.595(3)	2.56217(4)
B	0.402115068(6)	0.3991(4)	0.3978(4)	0.399(2)	0.396(1)	0.3992(7)	0.402 (1)	0.39934(1)
C	0.347444202(6)	0.3464(2)	0.3459(2)	0.344(2)	0.3508(6)	0.3436(4)	0.340(1)	0.34498(1)
V_{13}						2.805(3)		
V_{23}						3.826(9)		
ν_0		3570.493(5)	3566.793(5)	3560.032(9)	3568.48(2)	3564.81(6)	3564.03(1)	3534.6869(2)

[a] See M. Winnewisser *et al.*[14] In interest of space, no ground state centrifugal distortion constants determined by Winnewisser are listed; they are, however, explicitly included in all PGOPHER fits to the observed spectra.
[b] Anharmonic resonance term not included in the Hamiltonian.
[c] Anharmonic resonance term included explicitly in the Hamiltonian.
[d] Under jet-cooled conditions, only low J,K_a levels in the excited states are observed ($J \leq 9$ and $K_a \leq 3$). Thus, the PGOPHER least-squares fits to the excited state manifolds have all been simplified to a rigid asymmetric top Hamiltonian with centrifugal distortion terms fixed at zero.

J_{K_a,K_c} rotational levels in the perturbed states, where the transition intensities are calculated by integrating areas under a transition. Once the mixing angle is obtained, the percentages of zero-order 1^1 and 2^17^1 components in a specific J_{K_a,K_c} rotational level can be calculated by square-modulus of the quantum amplitudes in Eq. (3) and Eq. (4). Results are summarized in Fig. 4, where term values and percentages of zero-order 1^1 and 2^17^1 character in the experimentally observed upper state accessed by the ν^+ and ν^- bands are presented visually. Fig. 4 makes it evident that many, if not most, of the observed rovibrational levels are significantly mixed with nearly ~50%:50% zero-order 1^1 and 2^17^1 character, especially for the $K_a = 2$ sub-manifold. Thus, it is difficult to unambiguously assign the upper states of these bands to either perturbed 1^1 or 2^17^1 states. Moreover, an explicit local rotational crossing is observed between $J = 5$ and 6 in the upper asymmetry splitting of $K_a = 1$ sub-manifold, signaled by a rapid reversal in the predominant 1^1 vs. 2^17^1 character of the corresponding rovibrational level.

Our analysis approach is therefore to (i) exclude the entire $K_a = 2$ sub-manifold and the upper asymmetry component of the $K_a = 1$ sub-manifold, and (ii) fit only the more weakly perturbed $K_a = 0$, 1 (lower asymmetry component), and $K_a = 3$ data. It should be noted that the $K_a = 3$ sub-manifolds are still appreciably mixed and difficult to assign (Fig. 4); however, the data included in such a fit helps constrain the upper state *A* rotational constant. In summary, our initial strategy is to include in the fit only transitions to rovibrational levels with >60% zero-order 1^1 or 2^17^1 character, and thereby obtain improved effective rotational constants with which to better identify and predict the local rotational crossings. Although these represent transitions to rovibrational levels with a clear *predominance* of zero-order 1^1 or 2^17^1 character, it is important to appreciate that these levels are still significantly mixed, with zero-order character typically between 60 and 70% (and never >70%). This reduced subset of ν^+ and ν^- transitions into the coupled 1^1 and 2^17^1 submanifolds are then fitted to a rigid Watson Hamiltonian without including anharmonic resonance interactions and with all centrifugal terms fixed at zero. The result is summarized in Table 3 and represents best estimates, thus far, of band origins and effective rotational constants for the mixed 1^1 and 2^17^1 manifolds. Standard deviations of the fits are 0.0006 cm^{-1} and 0.0026 cm^{-1}, respectively, i.e., 10-fold improved and much closer to experimental uncertainty. Nevertheless, it should be noted that (i) the local rotational crossing in the upper asymmetry splitting of $K_a = 1$ sub-manifold is not well reproduced and (ii) the $K_a = 2$ sub-manifolds of 1^1 and 2^17^1 are still too far apart (~3.6 cm^{-1}) to be heavily mixed based on Fig. 4. We will return to this issue later in Section 4.1 and 4.2, where a more flexible 3-state rovibrational deperturbation analysis is attempted.

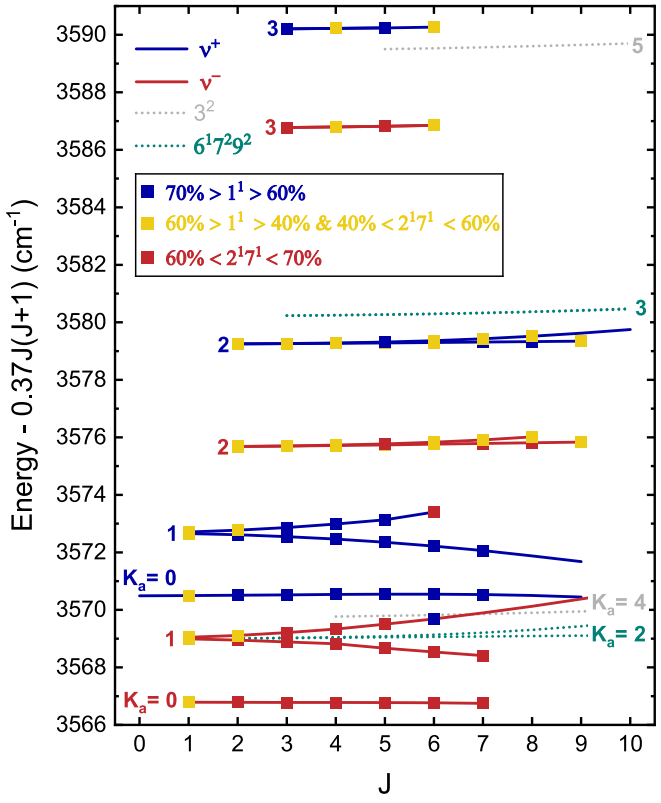

Fig. 4. Term values (corrected for $\bar{B}$ rotational constant) of upper states involved in the four observed rovibrational bands, with K_a assignments labeled. ν^+ (solid indigo line) and ν^- (solid dark red line) are computed from assigned transitions in this work and ground state rotational constants from Winnewisser *et al.* [14] The 3^2 (dot light gray line) and $6^17^29^2$ (dot teal line) levels are from PGOPHER predictions based on experimental rotational constants in Table 3. Filled squares of different colors indicate the percentages of zero-order 1^1 and 2^17^1 state composition for each of rovibrational level in ν^+ and ν^- manifold, with indigo for predominantly zero-order 1^1, dark red for predominantly zero-order 2^17^1, and yellow for a nearly 50%:50% mixture of the two zero-order states. (For interpretation of the references to colour in this figure legend, the reader is referred to the web version of this article.)

3.2. An additional red-shifted *a*-type band: The carbonyl stretch overtone ($2\nu_3$)

In the midst of this spectral complexity, a 6-fold weaker rovibrational band ~35 cm^{-1} to the red of ν^+ and ν^- bands is also observed in our jet-cooled spectrum. As evident in the overview scan in Fig. 3, the band structure is *a*-type, with closely spaced (but still well resolved) Q-branch features centered around ~3534.7 cm^{-1} (Fig. 5). We can readily assign 66 transitions, with a total of 39 different upper states measured ($0 \le J' \le 7$ and $0 \le K_a' \le 3$) and frequencies of the assigned transitions provided in SI. In sharp contrast to what was observed for the strongly coupled ν^+ and ν^- bands, transitions in this *a*-type rovibrational band fit extremely well to a simple rigid asymmetric top Watson Hamiltonian ($\sigma = 0.0008$ cm^{-1}, i.e., comparable to our experimental uncertainty), with the results summarized in Table 3. The fitted band origin at 3534.6869(2) cm^{-1} is now in excellent agreement with previous Raman jet spectroscopic work at 3533 cm^{-1} [29] and predictions from experimental diagonal and off-diagonal vibrational anharmonicities [27], for which a near perfect match with the C=O stretch first overtone ($2\nu_3$) at 3535.1 cm^{-1} is obtained. By way of additional support, the theoretical value for the $2\nu_3$

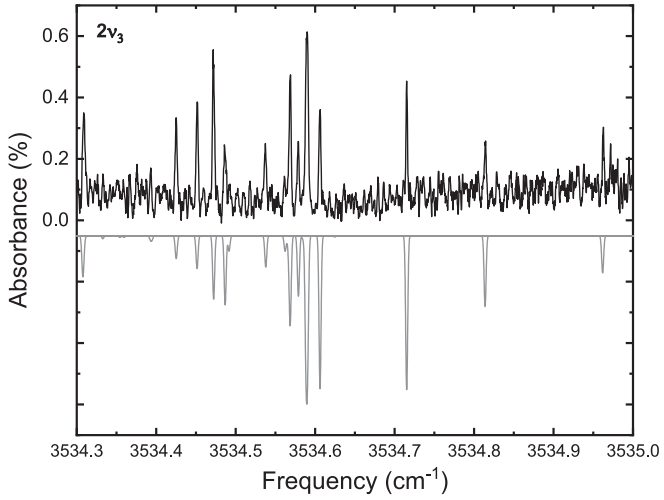

Fig. 5. Details of *a*-type Q-branch in the $2\nu_3$ C=O stretching first overtone. PGOPHER simulations (downward, gray), which is in good agreement with the experimental absorption spectrum (upward, black), are based on rotational constants in Table 3, rotational temperature of 10.9 K and a Gaussian linewidth of 70 MHz.

anharmonic (VPT2) frequency predicted from CCSD(T)/ANO2 levels of theory is 3539.361 cm^{-1}, also in close agreement with observation. Moreover, based on transition dipole moment vector expectations along the C=O bond (Fig. 1), one predicts a predominantly *a*-type band structure, again supporting assignment to the first overtone of the carbonyl stretch. Finally, in rotationally resolved He droplet studies [28], a band at 3532.74(4) cm^{-1} was observed and assigned to $2\nu_3$. This value is only quite modestly (~1.9 cm^{-1}) red shifted from the gas phase experimental value, also consistent with a $2\nu_3$ assignment.

If we combine our $2\nu_3$ band origin, $\tilde{\nu}(2\nu_3)$, with previously determined values for ν_3 and $3\nu_3$ [27], effective vibrational constants can be obtained from a Birge-Sponer plot,

$$\tilde{\nu}(n\nu_3) = \tilde{\omega}_e n - \tilde{\omega}_e x_e \left(n^2 + n\right) \tag{9}$$

yielding $\tilde{\omega}_e$ = 1795.3(3) cm^{-1} and x_e=0.00517(4) for harmonic vibrational frequency and diagonal anharmonicity, respectively. Finally, assuming a Dunham expression, the rotational constants of the $\nu_3 = n$ states X_n (for $X = A, B, C$) and the quantum number n are related to each other by:

$$X_n = X_g - {}^{i}\alpha_e^{(X)}\, n \tag{10}$$

where X_g is the ground state rotational constants and ${}^{i}\alpha_e^{(X)}$ corresponds to the vibration-rotation coupling constants of ν_i mode (i = 3). Based on experimentally determined A_n, B_n, C_n rotational constants of ground 3^0 [14], 3^1 [16], and 3^2 (present work) states, the vibration-rotation constants ${}^{3}\alpha_e^{(A)}$, ${}^{3}\alpha_e^{(B)}$, and ${}^{3}\alpha_e^{(C)}$ are found to be 0.0117(6), 0.00139(3), and 0.001230(6) cm^{-1}, respectively. These values agree well with our CCSD(T)/ANO2 calculations, where ${}^{3}\alpha_e^{(A)}$, ${}^{3}\alpha_e^{(B)}$, and ${}^{3}\alpha_e^{(C)}$ are computed to be 0.0122, 0.0014, and 0.0012 cm^{-1}. The evolution of these rotational constants with ν_3 quanta excitation is summarized in Fig. 6, illustrating excellent agreement with the smooth linear trend in overtone quantum number anticipated from a Dunham model.

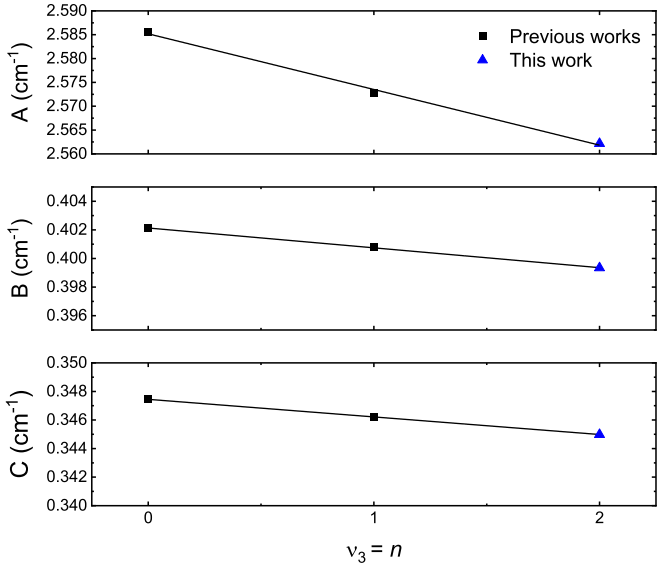

Fig. 6. *Trans*-HCOOH (Top) *A* (Middle) *B* (Bottom) *C* rotational constant progression upon *n* quanta excitation in ν_3. Ground state constants (ν_3 = 0) from previous microwave work [14] and ν_3 = 1 constants from previous FTIR work [16] (black squares) are plotted along with constants obtained in this work (blue triangles). The linear fit is based on expectations for a Dunham expansion model. (For interpretation of the references to colour in this figure legend, the reader is referred to the web version of this article.)

4. Discussion

4.1. Extending the 2 × 2 rovibrational deperturbation analysis

In Section 3.1, a 2 × 2 Hamiltonian was constructed, and the mixing angles for each of the J_{K_a,K_c} rotational level involved in ν^+ and ν^- bands were calculated. The Fermi resonance parameter β and energy separation between the zero-order states ΔE are related to the mixing angle and energy separation between the perturbed states by Eq. (5) and (2), for which we therefore have enough equations to solve. However, instead of solving for these two terms in each of the ν^+ and ν^- rotational manifolds, we can also pursue a simpler approach to vibrational deperturbation analysis. Specifically, the *integrated intensities* of the two rovibrational bands can instead be used to specify the mixing angle, θ, which with the observed band origins can then be solved for the anharmonic coupling parameter β and energy difference ΔE between the zero-order vibrational ν_1 and (ν_2 + ν_7) states. To obtain the integrated intensity of a rovibrational band, a rotational Boltzmann analysis of the experimental transition intensities is performed. Since all *a*- and *b*-type transitions arise from the same *trans*-HCOOH ground state manifold with identical populations, the full data set for both *a*/*b*-type and ν^+ and ν^- bands can be fit to a common slope ($-1/kT_{rot}$) with different intercepts (see Fig. 7). From analysis of these intercepts, we obtain an intensity ratio of $I_{(\nu_2+\nu_7)}'/I_{\nu_1}' = 0.64(6) = tan^2(\theta)$ for both *a*- and *b*-type sub-bands, corresponding to a mixing angle $\theta \approx 40(1)^\circ$ between the two zero-order states. Based on θ and energy difference $\Delta E' = 3.700(7)$ cm^{-1} (see Table 3), we can therefore infer an off-diagonal coupling matrix element of $\beta = 1.8(2)$ cm^{-1} and $\Delta E = 0.8(4)$ cm^{-1} for the energy difference between the zero-order vibrational states. This value of β is in reasonable agreement with prediction of $\beta \approx 1$ cm^{-1} in previous work by Nejad and Sibert [29]. The proximity of $\theta \approx 40(1)^\circ$ to 45° indicates that the perturbed bright 1^1

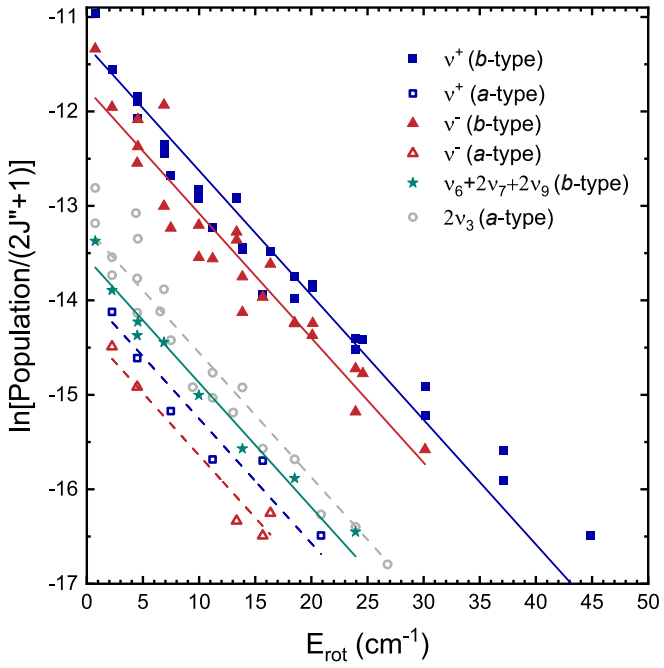

Fig. 7. Boltzmann plot for transition intensities in the ν^+ (indigo), ν^- (dark red), $2\nu_3$ (light gray), and $\nu_6 + 2\nu_7 + 2\nu_9$ (teal) bands. Filled markers are data from *b*-type sub-bands while open markers are for *a*-type sub-bands. Solid and dash lines represent linear fits to the data sets, with a global rotational temperature T_{rot} = 10.9(5) K determined. Displacements of the y-intercepts are related to integrated intensity ratios between the sub-bands. Note that the intensity ratio of ν^+, ν^-, and $\nu_6 + 2\nu_7 + 2\nu_9$ is 1.00:0.64:0.11, which is in excellent agreement with previous Raman spectroscopic studies [29]. (For interpretation of the references to colour in this figure legend, the reader is referred to the web version of this article.)

state reflects a highly mixed combination of zero-order states, specifically $(59\%)^{0.5}\ \varphi_{1^1}^0 + (41\%)^{0.5}\ \varphi_{2^1 7^1}^0$ and as emphasized in Section 3.1.

With this improved characterization of the anharmonic resonance, we can now attempt a more refined local rotational deperturbation analysis in PGOPHER, where the resonance interaction is explicitly included in the Watson Hamiltonian. In such an analysis, the values of β and zero-order vibrational band origins of 1^1 and $2^1 7^1$ states are fixed at the values computed above, with the rotational constants floated (all centrifugal terms fixed at zero). Furthermore, we now include transitions to both strongly perturbed upper asymmetry split states in the $K_a = 1$ manifolds as well as the $K_a = 2$ manifold. As one measure of success, such a local least-squares fitting exercise predicts an energy reversal in the zero-order vibrational state assignment for the entire $K_a = 3$ manifold. Nevertheless, such least-squares results are still only partially satisfactory, with standard deviations of the fit 10 times larger than experimental measurement uncertainties. In addition, a suspiciously large and unphysical K_a-dependent centrifugal distortion correction to β (i.e., $\beta^{eff} = \beta + \beta^{(D)} K_a^2$, where $\beta^{(D)} = -0.0128(3)$) is required for the convergence of the least-squares fits.

4.2. 3-State vibrational deperturbation analysis

One reason for lack of complete success in the above 2-state approach is our assumption of only anharmonic coupling between zero-order 1^1 and $2^1 7^1$ states and complete neglect of 3rd state coupling with the nearby $6^1 7^2 9^2$ state. Indeed, there is even direct experimental evidence for such 3rd state coupling from Raman jet spectroscopy [29], for which the $6^1 7^2 9^2$ state shifts to 4 cm^{-1} higher energy (3559(1) cm^{-1} ➔ 3563(1) cm^{-1}) upon *trans*-HCOOH to DCOOH deuteration (i.e., redshifting $2^1 7^1$ by ~900 cm^{-1}). This would be consistent with the $6^1 7^2 9^2$ state in *trans*-HCOOH already being pushed to lower energy ($\Delta\nu = -4(1)$ cm^{-1}) by level repulsion with the $2^1 7^1$ state. In order to allow for more complex coupling interactions, we have taken our spectral assignment/deperturbation analysis one step further to include three-state mixing based on the insightful treatment of Konen *et al.* [38]. Specifically, we assume that the only oscillator strength arises from the zero-order 1^1 state (denoted as $|1\rangle$), which is then perturbed by the zero-order dark states ($|2\rangle$ and $|3\rangle$ assigned to either $2^1 7^1$ or $6^1 7^2 9^2$) through a rotationless anharmonic resonance. The resulting 3×3 Hamiltonian:

$$\boldsymbol{H} = \begin{pmatrix} E_1 & V_{12} & V_{13} \\ V_{21} & E_2 & V_{23} \\ V_{31} & V_{32} & E_3 \end{pmatrix} \tag{11}$$

has diagonal elements E_i as zero-order energies of $|i\rangle$ and the off-diagonal terms $V_{ij} = V_{ji}$ as coupling between the 3 zero-order states. General solution to the Hamiltonian eq. $\mathbf{H}|\lambda\rangle = E_\lambda|\lambda\rangle$ ($\lambda = \alpha, \beta, \gamma$) yields a unitary matrix $\boldsymbol{U}$ of eigenvectors and a diagonal matrix $\boldsymbol{\Lambda}$ of eigenvalues,

$$\boldsymbol{U} = \begin{pmatrix} u_{1\alpha} & u_{1\beta} & u_{1\gamma} \\ u_{2\alpha} & u_{2\beta} & u_{2\gamma} \\ u_{3\alpha} & u_{3\beta} & u_{3\gamma} \end{pmatrix} \tag{12}$$

$$\boldsymbol{\Lambda} = \begin{pmatrix} E_\alpha & 0 & 0 \\ 0 & E_\beta & 0 \\ 0 & 0 & E_\gamma \end{pmatrix} \tag{13}$$

where the columns of $\boldsymbol{U}$ reflect the true molecular eigenstates ($|\alpha\rangle$, $|\beta\rangle$, and $|\gamma\rangle$) expanded in zero-order $|i\rangle$, with perturbed eigenenergies (E_α, E_β, and E_γ) matching the experimental band origins in Table 3. If only the $|1\rangle$ "bright" state carries oscillator strength, the top row of $\boldsymbol{U}$ is simply $(u_{1\alpha}, u_{1\beta}, u_{1\gamma}) = (0.76, 0.60, 0.25)$, where the normalized amplitudes (up to an arbitrary phase factor) are obtained from square root of the intensity ratios from Boltzmann analysis. Similarly, the lower 2 rows of $\boldsymbol{U}$ represent mutually orthogonal vectors ($|2\rangle$ and $|3\rangle$) which span a Hilbert space normal to $|1\rangle$ and readily obtained by Gram-Schmidt orthogonalization [38,39]. Given any one such solution for $|2\rangle$ and $|3\rangle$, all possible solutions for $\boldsymbol{U}$ for the remaining two rows can then be characterized (up to overall phase factors) by a rotation angle ϕ,

$$\boldsymbol{U}(\phi) = \begin{pmatrix} u_{1\alpha} & u_{1\beta} & u_{1\gamma} \\ 0 & 0 & 0 \\ 0 & 0 & 0 \end{pmatrix} + cos(\phi) \begin{pmatrix} 0 & 0 & 0 \\ \tilde{u}_{2\alpha} & \tilde{u}_{2\beta}\tilde{u}_{2\gamma} & \tilde{u}_{3\alpha}\tilde{u}_{3\beta}\tilde{u}_{3\gamma} \end{pmatrix} + sin(\phi) \begin{pmatrix} 0 & 0 & 0 \\ \tilde{u}_{3\alpha} & \tilde{u}_{3\beta}\tilde{u}_{3\gamma} - \tilde{u}_{2\alpha} - \tilde{u}_{2\beta} - \tilde{u}_{2\gamma} \end{pmatrix} \tag{14}$$

The full desired 3×3 Hamiltonian can be easily reconstructed by the matrix equation $\boldsymbol{H} = \boldsymbol{U}\boldsymbol{\Lambda}\boldsymbol{U}^\dagger$, with Eq. (14) being used to predict *all possible solutions* for diagonal (E_i) and off-diagonal (V_{ij}) matrix elements of $\boldsymbol{H}$ consistent with the spectra as a function of angle ϕ (see Fig. 8). As there are 6 independent variables (E_1, E_2, E_3) and (V_{12}, V_{13}, V_{23}) in $\boldsymbol{H}$ but only 5 constraints from the spectra (i.e., 3 band origins and 2 relative intensities), we can go no further without additional information or assumptions. We consider two such cases below.

The simplest assumption is $V_{23} = 0$, which treats the zero-order dark states as "pre-diagonalized" and is equivalent to the well-known Lawrance and Knight algorithm [40] for obtaining coupling matrix elements in an N-state system from N band origins and N-1 relative intensities. However, as discussed above, Raman spectroscopy with CH/CD isotopic substitution clearly reveals significant coupling between zero-order "dark" $2^1 7^1$ and $6^1 7^2 9^2$ states, which therefore requires $V_{23} \neq 0$. Alternate specification of bright state coupling with either of the two dark states (V_{12} or V_{13}) is equivalent (see Fig. 8) to determining ϕ and thus all matrix elements of $\boldsymbol{H}$. Indeed, the choice of $V_{13} = 0$ (or equivalently $V_{12} = 0$) in nitric acid was taken by Stanton and coworkers and rationalized by *ab initio* calculation of the relevant matrix elements. Once again, small Raman shifts (≈1 cm^{-1}) in the 1^1 state from HCOOH/DCOOH spectroscopy provide some insight, specifically that V_{12} is small and possibly negligible. If we assume $V_{12} = 0$ (or $V_{13} = 0$), the four possible solutions for matrix elements of $\boldsymbol{H}$ are marked with four vertical lines in Fig. 8, with E_2 and E_3 interchanged for $V_{12} = 0$ and $V_{13} = 0$ and off-diagonal coupling terms differing only by relative sign. For choice of non-zero off-diagonal terms of the same sign, the resulting Hamiltonian is,

$$\boldsymbol{H} = \begin{pmatrix} 3568.48(2) & 0 & 2.805(3) \\ 0 & 3564.81(6) & 3.826(9) \\ 2.805(3) & 3.826(9) & 3564.03(1) \end{pmatrix} \tag{15}$$

with all terms in cm^{-1} and standard deviations derived from experimental intensity uncertainties. It is worth emphasizing that such a 3-state treatment assuming negligible coupling between zero-order 1^1 and $2^1 7^1$ explains the IR spectra equally well but makes rather different predictions from our 2-state analyses of which states couple weakly or strongly.

We again attempt refined rotational deperturbation analysis using PGOPHER, where all zero-order energies and coupling terms are fixed at the computed values in Eq. (15) and rotational constants are floated (all centrifugal terms fixed at zeros). Least-squares fitting results are summarized in Table 3. Unlike the previous two-state system, no centrifugal distortion correction needs to be added to the coupling terms for the fit

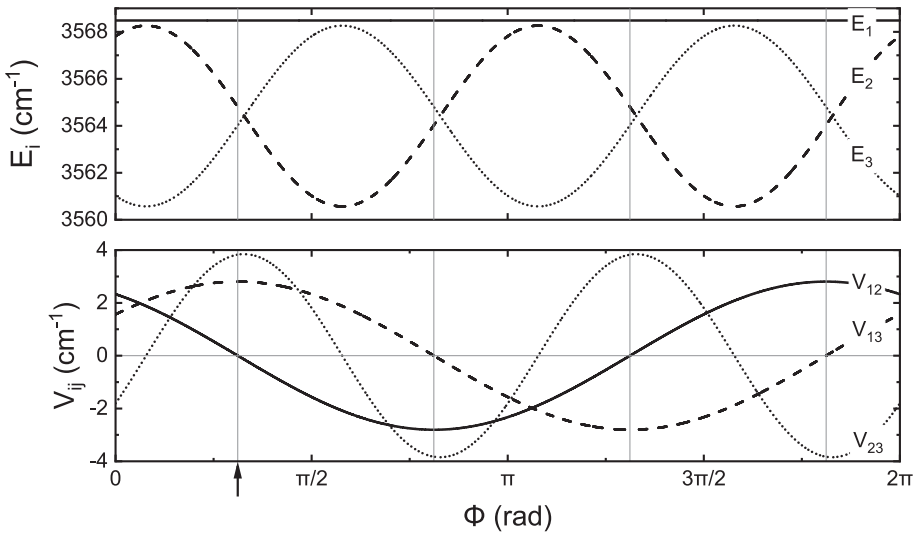

Fig. 8. Values of zero-order energies (E_i) and Fermi resonance coupling constants (V_{ij}) as a function of angle ϕ. Four possible solutions under the constraints that either V_{12} or V_{13} is zero are shown as vertical lines.

to converge (and adding them does not improve the fit). Fig. 9 shows the experimental spectrum for the selected *b*-type Q-branch region, with PGOPHER predictions based on no coupling, 2-state system, and 3-state system plotted downwards for comparison. A reversal in the $K_a = 3$ manifold assignments of the 1^1 and $2^1 7^1$ states is also found.

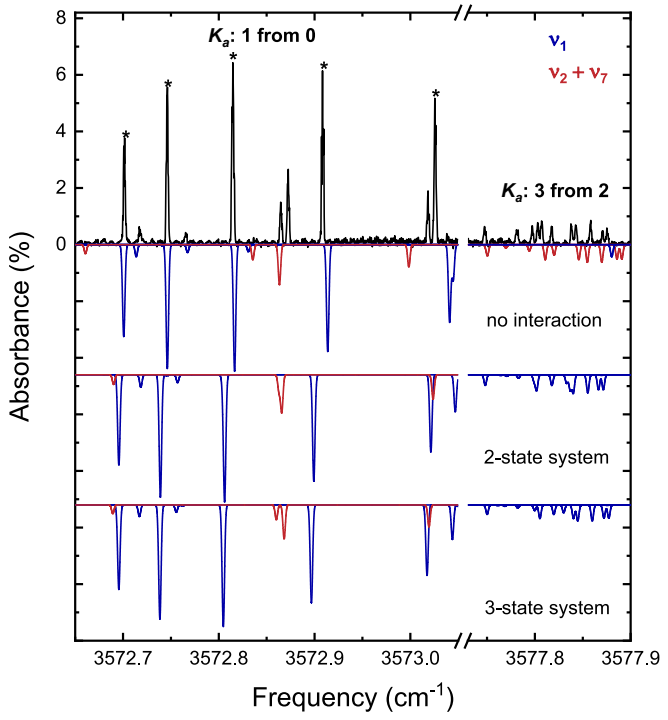

Fig. 9. Detailed experimental spectrum showing *b*-type K_a: $1 \leftarrow 0$ and $3 \leftarrow 2$ Q-branches of the ν^+ and ν^- bands, respectively. Non-overlapping K_a: $1 \leftarrow 0$ progressions in ν^+ are marked with asterisks (for $J = 1$ to 5). PGOPHER simulations using rotational constants obtained under different models are plotted downwards: (top panel) no interaction between the 1^1, $2^1 7^1$, and $6^1 7^2 9^2$ states; (middle panel) Fermi interaction between the 1^1 and $2^1 7^1$ states; (bottom panel) anharmonic resonance interaction between the 1^1 and $6^1 7^2 9^2$ states + anharmonic resonance interaction between $2^1 7^1$ and $6^1 7^2 9^2$ states. Note that for the "no interaction" model, intensities of the dark state bands are based on experimental values while intensities of the zero-order dark state bands are fixed at zero in the 2-state and 3-state system.

Additionally, one success of our three-state analysis is that when the zero-order energy of $2^1 7^1$ is red-detuned by ~900 cm^{-1}, the predicted band origins of 1^1 and $6^1 7^2 9^2$ states (3569.8381 cm^{-1} and 3562.6733 cm^{-1}) agree well with results from previous C–D substitution studies of *trans*-HCOOH [29], for which the perturbed 1^1 and $6^1 7^2 9^2$ band origins become 3569 cm^{-1} and 3563 cm^{-1}, respectively (see Fig. S1). However, it is important to note that standard deviation of the fit does not improve much and is still in 10×excess of the frequency uncertainties. Nevertheless, our results do permit first high-resolution spectroscopic constants to be obtained for the three states, which should provide help in a more complete assignment analysis of room temperature FTIR spectra from the Herman group [23].

Finally, the *A*, *B*, and *C* rotational constants of zero-order 1^1 state from such least-squares fits using a three-state system, plotted in Fig. 10 along with results from previous works [23,24], are especially revealing. We notice that the averages of rotational constants of zero-order 1^1 and $2^1 7^1$ states follow well with the Dunham expression. The *A* rotational constant clearly depends most sensitively to quanta ($v_1 = n$) in the OH stretch ($^1\alpha_e^{(A)}$= 0.0135(2) cm^{-1}), while $\alpha_e^{(B)}$ and $\alpha_e^{(C)}$ are 2–3 orders of magnitude less sensitive ($^1\alpha_e^{(B)}$ = 3(1)×10^{-4} and $^1\alpha_e^{(C)}$ = 9(4)×10^{-5} cm^{-1}). This is of course consistent with physical expectation, as the OH stretch vibrational coordinate is nearly perpendicular to the *a*-axis. Thus, modest increase in the vibrationally averaged OH bond length upon excitation results in significant increase in the *a*-axis moment of inertia, resulting in a Dunham-like linear decrease in *A* rotational constant with quanta of v_1.

4.3. Rotation of OH stretching transition dipole moment direction

Based on the rotational Boltzmann analysis for *a*- and *b*-type transitions in ν^+ and ν^-, the fitted *a*- to *b*-type band intensity ratios are both found to be ~0.080(8). We can extend this further by comparison with rovibrational intensity predictions from a simple bond-dipole model, where the transition dipole moment $\boldsymbol{\mu}$ arises from normal mode ($\boldsymbol{q}$) displacements $\boldsymbol{r_i}$ of static polarization charges q_i on atom *i* (i.e., $\partial\boldsymbol{\mu}/\partial\boldsymbol{q} \approx \sum_i q_i \partial \boldsymbol{r}_i/\partial\boldsymbol{q}$). For pure stretching of the OH bond (7.6° away from the *b* axis), the theoretical *a*- to *b*-type intensity ratio would be,

$$\left(\frac{I_a}{I_b}\right)_{bond-dipole} = \left(\frac{|\partial\boldsymbol{\mu}_a/\partial\boldsymbol{q}|}{|\partial\boldsymbol{\mu}_b/\partial\boldsymbol{q}|}\right)^2 = \left(\frac{sin(7.6^\circ)}{cos(7.6^\circ)}\right)^2 = 0.018 \quad (16)$$

This is dramatically (~450%) smaller than experimentally observed, which signals an additional rotation of the transition dipole moment

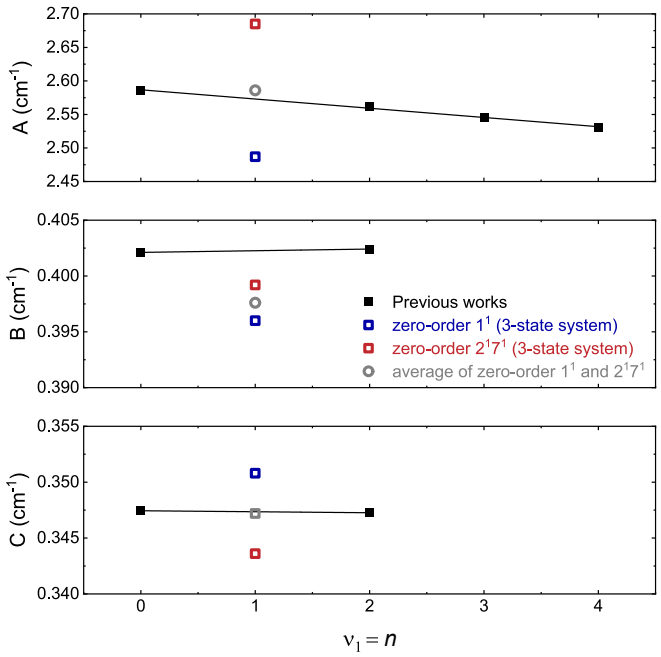

Fig. 10. Systematic evolution of experimentally determined *trans*-HCOOH (Top panel) *A* (Middle panel) *B* (Bottom panel) *C* rotational constants upon *n* quanta excitation in the ν_1 OH stretching mode (black) [23]. It should be noted that for $\nu_1 = 3$, the *A* value was deduced by using the Q-heads provided by Bauer and Badger [23,46] while numerical values for *B* and *C* constants are used [23]. The linear fit is based on an effective linear Dunham expansion model, where the slope is the vibration-rotation constant, and the y-intercept ($\nu_1 = 0$) is the experimental ground state rotational constant [14]. Notice that the averaged rotational constants for the two mixed states follows a linear Dunham progression reasonably well over the full overtone series, particularly for A, C.

towards the *a* axis. Geometrically stated, the experimentally determined intensity ratio predicts $\partial\boldsymbol{\mu}/\partial\boldsymbol{q}$ to point $\pm 15.9(8)^\circ$ away from the *b* axis, corresponding to either $|7.6^o \pm 15.9^o| = 23.5^\circ$ clockwise or 8.3° counterclockwise rotation toward the *a*-axis (see Fig. 1).

Such a rotation of the transition dipole moment direction could arise from several different sources. One such contribution would be from vibrational "charge-sloshing" effects [41,42], arising from vibrationally mediated flow of π-electron density from the C=O carboxyl group toward the adjacent O atom upon stretching of the OH bond, which leads to an additional electrical anharmonicity term in transition dipole moment (i.e., $\sum_i \boldsymbol{r}_i \partial q_i/\partial \boldsymbol{q}$). Indeed, in the limit of vibrational removal of the acidic proton from OH, this would physically correspond to complete resonance delocalization of electrons in the formate anion ($HCOO^-$), which would certainly lead to enhancement of the *a*-type band intensity. Similar deviations were also noted in previous high-resolution IR study of the OH stretching band in the *cis*-formic acid conformer [20], which were also explained by such a vibrationally-induced *delocalization of the electron wavefunction amplitudes*. However, an equally plausible explanation could be vibrationally-induced *proton transfer* to the O atom on the carboxyl group upon stretching of the acidic OH bond. Indeed, this is the mechanism proposed by Hurtmans *et al.*, based on experimental spectra for the series of OH stretching overtone bands from $\nu_1 = 1$ to 4 [23]. By way of support, their *ab initio* calculations predict a continuous counter-clockwise rotation of the transition dipole moment towards the *a* axis. Table 4 summarizes the evolution of experimental transition dipole moment direction with $\nu_1 = n$ quanta excitation, providing additional evidence for such an interpretation.

5. Conclusion

In this work, first high-resolution IR absorption spectra of jet-cooled *trans*-formic acid in the ν_1 region between 3528 and 3583 cm^{-1} are presented. Two *a*/*b*-type, one *b*-type, and one *a*-type rovibrational bands are found and assigned to ν^+ (3570.493 cm^{-1}), ν^- (3566.793 cm^{-1}), ($\nu_6 + 2\nu_7 + 2\nu_9$) (3560.032 cm^{-1}), and $2\nu_3$ (3534.6869 cm^{-1}), respectively, where ν^+ and ν^- are mixtures of ν_1 and ($\nu_2 + \nu_7$). This is already surprising, as the predicted harmonic density of states is only $\approx 0.09/cm^{-1}$ in this region [43–45], which implies that the additional rovibrational bands must arise from a statistically unlikely (but nevertheless quite evident!) resonance between the zero-order bright 1^1 state and nearby dark states. While the $2\nu_3$ *a*-type and ($\nu_6 + 2\nu_7 + 2\nu_9$) *b*-type rovibrational bands can be well fit to a rigid Watson Hamiltonian, transitions to the ν^+ and ν^- manifolds are only poorly fit even with quartic centrifugal distortion constants included. We argue that this is due to localized rotational crossings between the zero-order 1^1 and 2^17^1 states.

Our first approach is therefore to obtain effective rotational constants by fitting transitions without including anharmonic resonance. We then take this one step further using a 2-state system, where only zero-order 1^1 and 2^17^1 states are coupled. However, this simplified model is only partially satisfactory due to complete neglect of the nearby $6^17^29^2$ state while there is direct evidence of the $2^17^1/6^17^29^2$ pair coupling from previous HCOOH/DCOOH work [29]. Therefore, a more refined 3-state system based on Stanton and coworkers is used [38]. The zero-order 1^1, 2^17^1, and $6^17^29^2$ states are computed to be at 3568.48(2), 3564.81(6), and 3564.03(1) cm^{-1}, respectively, with anharmonic resonance coupling constants for the $1^1/6^17^29^2$ and $2^17^1/6^17^29^2$ interaction being 2.805(3) and 3.826(9) cm^{-1}. One success of our three-state analysis is the correct prediction of both HCOOH/DCOOH spectra. Nevertheless, complete fits of the observed spectrum down to our reduced-Doppler experimental uncertainty levels has yet to be achieved. It is our hope that the spectroscopic constants from the present much colder, reduced-Doppler study will aid further a more complete assignment and analysis of the extensive room temperature spectra by Herman and coworkers [23].

Finally, the deviation between the experimentally determined relative *a*- to *b*-type sub-band intensity of the ν_1 band and simple bond-dipole model predictions signals a rotation of transition dipole moment direction away from *b* axis. This rotation can arise from resonance delocalization of electron amplitude from the C=O group along the formate OCO^- chain (i.e. vibrational charge-sloshing effects) or proton transfer to the other O atom upon excitation of the OH stretch.

Table 4
Evolution of experimentally determined OH stretching mode transition dipole moment direction with *n* quanta excitation in ν_1. φ is the angle between *b* principal rotation axis and transition dipole moment direction.

$\nu_1 = n$	φ (°)
1	18
2[a]	32
3	–
4[a]	46

[a] See D. Hurtmans *et al.*[23].

Author statement

David Nesbitt Conceptualization, Methodology, Writing- Reviewing and Editing

Ya-Chu Chan Data Collection, Analysis, Writing-Reviewing and Editing

Declaration of Competing Interest

The authors declare that they have no known competing financial interests or personal relationships that could have appeared to influence

the work reported in this paper.

Data availability

Data will be made available on request.

Acknowledgements

This work has been supported by grants from the Department of Energy (DE-FG02-09ER16021), with initial funds for construction of the slit-jet laser spectrometer provided by the National Science Foundation (CHE 1665271/2053117, PHY 1734006). We would like to express our deepest appreciation to the late Prof. Colin Western Bristol for development of the PGOPHER spectroscopic predictor/fitting program suite, without which the present analysis of *trans*-formic acid infrared spectra would have been extremely challenging if not impossible. Colin's rapid email responses, gentle guidance, and ever patient help with young enthusiastic spectroscopists (as well as faltering faculty members!) has had a profound impact on the world of high-resolution spectroscopy. His brilliance, calm presence, and quiet humility will be sorely missed.

Appendix A. Supplementary data

Supplementary data to this article can be found online at https://doi.org/10.1016/j.jms.2023.111743.

References

[1] A. Goldman, F. Murcray, D. Murcray, C. Rinsland, A search for formic acid in the upper troposphere: A tentative identification of the 1105-cm^{-1} ν_6 band Q branch in high-resolution balloon-borne solar absorption spectra, Geophys. Res. Lett. 11 (4) (1984) 307–310.
[2] D.B. Millet, M. Baasandorj, D.K. Farmer, J.A. Thornton, K. Baumann, P. Brophy, S. Chaliyakunnel, J.A. de Gouw, M. Graus, L. Hu, A large and ubiquitous source of atmospheric formic acid, Atmos. Chem. Phys. 15 (11) (2015) 6283–6304.
[3] E. Willemot, D. Dangoisse, N. Monnanteuil, J. Bellet, Microwave spectra of molecules of astrophysical interest. XVIII, Formic acid, J. Phys. Chem. Ref. 9 (1) (1980) 59–160.
[4] H. Chaabouni, S. Baouche, S. Diana, M. Minissale, Reactivity of formic acid (HCOOH) with H atoms on cold surfaces of interstellar interest, Astron. Astrophys. 636 (2020) A4.
[5] S.-Y. Liu, D.M. Mehringer, L.E. Snyder, Observations of formic acid in hot molecular cores, Astrophys. J. 552 (2) (2001) 654.
[6] B. Zuckerman, J.A. Ball, C.A. Gottlieb, Microwave detection of interstellar formic acid, Astrophys. J. 163 (1971) L41.
[7] G. Winnewisser, E. Churchwell, Detection of formic acid in Sagittarius B2 by its 2_{11}-2_{12} transition, Astrophys. J. 200 (1975) L33–L36.
[8] W.M. Irvine, P. Friberg, N. Kaifu, H. Matthews, Y. Minh, M. Ohishi, S. Ishikawa, Detection of formic acid in the cold, dark cloud L134N, Astron. Astrophys. 229 (1990) L9–L12.
[9] D. Bockelée-Morvan, D. Lis, J. Wink, D. Despois, J. Crovisier, R. Bachiller, D. Benford, N. Biver, P. Colom, J. Davies, New molecules found in comet C/1995 O1 (Hale-Bopp). Investigating the link between cometary and interstellar material, Astron. Astrophys. 353 (2000) 1101–1114.
[10] W.H. Hocking, The other rotamer of formic acid, *cis*-$HCOOH^1$, Z. Naturforsch. A 31 (9) (1976) 1113–1121.
[11] S. Cuadrado, J.R. Goicoechea, O. Roncero, A. Aguado, B. Tercero, J. Cernicharo, Trans-cis molecular photoswitching in interstellar space, Astron. Astrophys. 596 (2016) L1.
[12] E. Bjarnov, W. Hocking, The Structure of the Other Rotamer of Formic Acid, *cis*-$HCOOH^{1,\ 2}$, Z. Naturforsch. A 33 (5) (1978) 610–618.
[13] J. Vander Auwera, High-resolution investigation of the far-infrared spectrum of formic acid, J. Mol. Spectrosc. 155 (1) (1992) 136–142.
[14] M. Winnewisser, B.P. Winnewisser, M. Stein, M. Birk, G. Wagner, G. Winnewisser, K.M. Yamada, S.P. Belov, O.I. Baskakov, Rotational spectra of *cis*-HCOOH, *trans*-HCOOH, and trans-$H^{13}COOH$, J. Mol. Spectrosc. 216 (2) (2002) 259–265.
[15] M. Takami, K. Shimoda, Microwave Spectrum of HCOOH in the v_{CH}= 1 Vibrational State Observed by Laser-Microwave Double and Triple Resonance, Jpn. J. Appl. Phys. 13 (11) (1974) 1699.
[16] W. Weber, P. Maker, J. Johns, E. Weinberger, Sub-Doppler laser-Stark and high-resolution Fourier transform spectroscopy of the ν_3 band of formic acid, J. Mol. Spectrosc. 121 (2) (1987) 243–260.
[17] R. Bumgarner, J.-I. Choe, S.G. Kukolich, R. Butcher, High-resolution spectroscopy of the ν_6 and ν_8 bands of formic acid, J. Mol. Spectrosc. 132 (1) (1988) 261–276.
[18] A. Perrin, J.-M. Flaud, B. Bakri, J. Demaison, O. Baskakov, S. Sirota, M. Herman, J. Vander Auwera, New high-resolution analysis of the ν_7 and ν_9 fundamental bands of *trans*-formic acid by Fourier transform infrared and millimeter-wave spectroscopy, J. Mol. Spectrosc. 216 (2) (2002) 203–213.
[19] O.I. Baskakov, V.-M. Horneman, J. Lohilahti, S. Alanko, High resolution FTIR spectra of the ν_9 vibrational band of *cis*-rotamers HCOOH and $H^{13}COOH$, J. Mol. Struct. 795 (1–3) (2006) 49–53.
[20] K.D. Doney, A. Kortyna, Y.-C. Chan, D.J. Nesbitt, Formation and detection of metastable formic acid in a supersonic expansion: High resolution infrared spectroscopy of the jet-cooled *cis*-HCOOH conformer, J. Chem. Phys. 156 (20) (2022), 204309.
[21] K.A. Meyer, M.A. Suhm, Stretching of *cis*-formic acid: warm-up and cool-down as molecular work-out, Chem. Sci. 10 (25) (2019) 6285–6294.
[22] E.M. Maçôas, J. Lundell, M. Pettersson, L. Khriachtchev, R. Fausto, M. Räsänen, Vibrational spectroscopy of *cis*-and *trans*-formic acid in solid argon, J. Mol. Spectrosc. 219 (1) (2003) 70–80.
[23] D. Hurtmans, F. Herregodts, M. Herman, J. Liévin, A. Campargue, A. Garnache, A. Kachanov, Spectroscopic and ab initio investigation of the ν_{OH} overtone excitation in *trans*-formic acid, J. Chem. Phys. 113 (4) (2000) 1535–1545.
[24] V. Svoboda, J. Rakovský, O. Votava, High-resolution spectra of $2\nu_{OH}$ overtone of *trans*-formic acid in the supersonic jet, J. Quant. Spectrosc. Radiat. Transf. 292 (2022) 108319.
[25] Y. Maréchal, IR spectra of carboxylic acids in the gas phase: A quantitative reinvestigation, J. Chem. Phys. 87 (11) (1987) 6344–6353.
[26] H. Morita, S. Nagakura, Near-infrared spectra of hydrogen-bonded cyclic dimers of some carboxylic acids, J. Mol. Spectrosc. 41 (1) (1972) 54–68.
[27] M. Freytes, D. Hurtmans, S. Kassi, J. Liévin, J. Vander Auwera, A. Campargue, M. Herman, Overtone spectroscopy of formic acid, Chem. Phys. 283 (1–2) (2002) 47–61.
[28] F. Madeja, P. Markwick, M. Havenith, K. Nauta, R. Miller, Rotationally resolved infrared spectroscopy of h_2-and d_1-formic acid monomer in liquid He droplets, J. Chem. Phys. 116 (7) (2002) 2870–2878.
[29] A. Nejad, E.L. Sibert III, The Raman jet spectrum of *trans*-formic acid and its deuterated isotopologs: Combining theory and experiment to extend the vibrational database, J. Chem. Phys. 154 (6) (2021), 064301.
[30] S. Davis, M. FarniK, D. Uy, D.J. Nesbitt, Concentration modulation spectroscopy with a pulsed slit supersonic discharge expansion source, Chem. Phys. Lett. 344 (1–2) (2001) 23.
[31] E. Riedle, S.H. Ashworth, J.T. Farrell, D.J. Nesbitt, Stabilization and precise calibration of a continuous wave difference frequency spectrometer by use of a simple transfer cavity, Rev. Sci. Instrum. 65 (1) (1994) 42.
[32] A.S. Pine, High-resolution methane ν_3 band spectra using a stabilized tunable difference-frequency laser system*, J. Opt. Soc. Am. 66 (2) (1976) 97.
[33] D.A. Matthews, L. Cheng, M.E. Harding, F. Lipparini, S. Stopkowicz, T.-C. Jagau, P. G. Szalay, J. Gauss, J.F. Stanton, Coupled-cluster techniques for computational chemistry: The CFOUR program package, J. Chem. Phys. 152 (21) (2020), 214108.
[34] J. Demaison, M. Herman, J. Liévin, Anharmonic force field of *cis*-and *trans*-formic acid from high-level ab initio calculations, and analysis of resonance polyads, J. Chem. Phys. 126 (16) (2007), 164305.
[35] D.P. Tew, W. Mizukami, Ab initio vibrational spectroscopy of *cis*-and *trans*-formic acid from a global potential energy surface, J. Phys. Chem. A 120 (49) (2016) 9815–9828.
[36] E.L. Sibert III, Theoretical studies of vibrationally excited polyatomic molecules using canonical Van Vleck perturbation theory, J. Chem. Phys. 88 (7) (1988) 4378–4390.
[37] C.M. Western, PGOPHER: A program for simulating rotational, vibrational and electronic spectra, J. Quant. Spectrosc. Radiat. Transf. 186 (2017) 221.
[38] I.M. Konen, E.X. Li, M.I. Lester, J. Vázquez, J.F. Stanton, Infrared overtone spectroscopy and vibrational analysis of a Fermi resonance in nitric acid: Experiment and theory, J. Chem. Phys. 125 (7) (2006), 074310.
[39] G. Strang, Linear algebra and its applications, Thomson, Brooks/Cole, Belmont, CA, 2006.
[40] W.D. Lawrance, A.E. Knight, Direct deconvolution of extensively perturbed spectra: the singlet-triplet molecular eigenstate spectrum of pyrazine, J. Phys. Chem. 89 (6) (1985) 917–925.
[41] E.S. Whitney, T. Haeber, M.D. Schuder, A.C. Blair, D.J. Nesbitt, High-resolution infrared studies in slit supersonic discharges: CH_2 stretch excitation of jet-cooled CH_2Cl radical, J. Chem. Phys. 125 (5) (2006), 054303.
[42] A.B. McCoy, T.L. Guasco, C.M. Leavitt, S.G. Olesen, M.A. Johnson, Vibrational manifestations of strong non-Condon effects in the $H_3O^+{\cdot}X_3$ (X = Ar, N_2, CH_4, H_2O) complexes: A possible explanation for the intensity in the "association band" in the vibrational spectrum of water, Phys. Chem. Chem. Phys. 14 (20) (2012) 7205.
[43] J. Barker, T. Nguyen, J. Stanton, C. Aieta, M. Ceotto, F. Gabas, T. Kumar, C. Li, L. Lohr, A. Maranzana, N. Ortiz, J. Preses, J. Simmie, J. Sonk, P. Stimac, in: J. R. Barker (Ed.), MultiWell-2022 software suite, University of Michigan, Ann Arbor, Michigan, USA, 2022.
[44] T. Beyer, D. Swinehart, Algorithm 448: number of multiply-restricted partitions, Commun. ACM 16 (6) (1973) 379.
[45] S.E. Stein, B. Rabinovitch, Accurate evaluation of internal energy level sums and densities including anharmonic oscillators and hindered rotors, J. Chem. Phys. 58 (6) (1973) 2438–2445.
[46] S.H. Bauer, R.M. Badger, The O–H band in the vapors of some organic acids and of tertiary amyl alcohol in the region λ9700, J. Chem. Phys. 5 (11) (1937) 852–855.